

Effect of sintering on structure of nanodiamond

G.N. Yushin^a, S. Osswald^a, V.I. Padalko^b, G.P. Bogatyreva^c, Y. Gogotsi^{a,*}

^aDepartment of Materials Science and Engineering and A. J. Drexel Nanotechnology Institute, Drexel University, Philadelphia, PA 19104, USA

^bALIT Inc., Kiev, 03067, Ukraine

^cV.N. Bakul Institute for Superhard Materials of the National Academy of Sciences of Ukraine, Kiev, 04074, Ukraine

Received 23 December 2004; accepted 23 June 2005

Available online 10 August 2005

Abstract

Recent successful industrial applications of ultra dispersed diamond have triggered additional scientific interest in its structure and surface properties, as well as changes in these properties upon various post-treatments. In this work, we report a systematic study of the structure of nanocrystalline diamond powder before and after sintering by using multi-wavelength Raman spectroscopy, high resolution transmission electron microscopy, and sorption measurements. Purified nanodiamond powder showed the presence of amorphous carbon and carbon onions and had a specific surface area of about 200 m²/g. Sintering performed for 3 min at 4.5–7 GPa of quasi-hydrostatic pressure at 1400 °C resulted in the decrease of sp² carbon content in the diamond sample, an increase in the average size of diamond grains, and noticeable broadening of the grain size distribution. Sintered nanodiamond retained a porous structure and demonstrated a specific surface area of about 135 m²/g. The produced material can be used as a fine abrasive powder, as a stationary phase in chromatography or as a durable bio-compatible membrane (filter) for bio-medical applications. This work demonstrated the successful sintering of nanodiamond and could be used for optimizing the production process of the porous nanocrystalline diamond with desired characteristics.

© 2005 Elsevier B.V. All rights reserved.

Keywords: 4: High resolution electron microscopy; 5: Vibrational properties; 6: Biomaterials; Cutting tools

1. Introduction

Diamond particles of 2–20 nm in size have attracted an increased attention in the past few years [1–4]. Nanodiamond, also called nanocrystalline diamond (NCD) powder, or ultra dispersed diamond (UDD), is considered a promising material for various applications, including abrasives for the semiconductor and optical industries, extra durable and hard coatings, additives to lubricants for engines and moving gears, polymer reinforcements, protein adsorbents, and even medicinal drugs [1,5–7]. Nanodiamond powders produced by detonation of explosives in a closed chamber have been commercially available in Russia and Ukraine for over 15 years, and most publications on this

topic originate from these countries (see [1–4] for reviews). Although most of the described applications require isolated nanodiamond particles, application of nanodiamonds in abrasives and cutting tools may also benefit from the utilization of sintered nanodiamond. Compared to microcrystalline diamond, sintered nanodiamond may provide a higher quality fine polishing of hard ceramics and optical components due to a rounded particle shape and more isotropic material properties. Sintering is also one of the very few ways to produce porous diamond. While porous diamond containing carbide-derived carbon [8] has very small pores of <1 nm, sintered nanodiamond may contain larger mesopores (pores >2 nm), that are useful for biological applications. Porous diamond produced by sintering may also have very little non-diamond phase content. Due to its excellent mechanical properties and the biocompatibility of diamond, sintered nanodiamond membranes may find applications in biotechnology, bioengineer-

* Corresponding author.

E-mail address: gogotsi@drexel.edu (Y. Gogotsi).

ing, and medicine. However, very little is known about sintering of UDD. Even the surface chemistry and phase composition of UDD is still poorly understood.

Transmission electron microscopy (TEM) is often used to determine the particle (or grain) size and structure of nanocrystalline materials. Raman spectroscopy is the most powerful and widely used method of studying diamond and other carbon allotropes. Its non-destructive nature combined with the ease of sample preparation, relatively short analysis time and large analyzed area needed for statistical measurements offers considerable advantages for UDD study. Raman features of nanodiamond are different from that of microcrystalline CVD diamond films or single crystals. Both the single crystalline and polycrystalline diamond with grain size above $\sim 20 \mu\text{m}$ show only one strong and narrow first-order peak at $\sim 1332 \text{ cm}^{-1}$ (triple-degenerated peak) [9,10] with the full width at half maximum (FWHM) of $\sim 1\text{--}3 \text{ cm}^{-1}$ [11]. With decreasing crystallite size to below a micrometer, the FWHM of this peak increases to the values of 10 cm^{-1} or more due to the decrease in the perfection of the crystal and the increase in the content of non-diamond phases in the sample [12]. UDD also show several additional Raman peaks, including peaks at ~ 500 [13], ~ 1090 [13], and $\sim 1600 \text{ cm}^{-1}$ [13,14]. It is worth noting that nanodiamond samples (either UDD or CVD grown) may show very weak or no Raman peak at $\sim 1332 \text{ cm}^{-1}$ due to strong vibrations from sp^2 bonded carbon along grain boundaries. Compared to visible Raman, UV-Raman analysis offers stronger diamond signal due to resonance enhancement [15] and thus relatively easy identification of nanodiamond.

In this paper, we studied structural changes in nanodiamond upon sintering by multi-wavelength Raman spectroscopy and TEM.

2. Experimental

UDD with a density of 3.2 g/cm^3 was produced at ALIT Inc. (Ukraine) by a detonation of trinitrotoluene explosives in a 100 m^3 chamber and subsequent chemical purification. Detonated samples were washed first in a 50% solution of a hydrochloric acid that was heated to $100 \text{ }^\circ\text{C}$ to remove metal impurities and then in a 50% solution of sulfuric and chromium (1:1) acids heated to $180\text{--}200 \text{ }^\circ\text{C}$ to remove graphite. Finally, samples were cleaned in de-ionized (DI) water to remove the remaining soluble residues. Auger and IR spectroscopic examination reported elsewhere [16] revealed oxygen and hydrogen-containing functional groups on the surface of the particles. Sintering of UDD was performed for 3 min at $1400 \text{ }^\circ\text{C}$ at a $4.5\text{--}7 \text{ GPa}$ of quasi-hydrostatic pressure at ALIT, Inc. Sintered material was crushed to a powder of $1\text{--}6 \mu\text{m}$ particle size, washed for 30 min in a 50% solution of sulfuric and chromium (1:1) acids and for 15 min in DI water. According to the provided specifications, sintered UDD exhibited a vickers hardness of

$\sim 10 \text{ GPa}$, and a density of $\sim 3 \text{ g/cm}^3$ as measured by a commercial glass pycnometer.

Argon adsorption on the samples was carried out using a Quantachrome Autosorb-1. Prior to the analysis, the diamond samples were outgassed in helium for 30 min at $60 \text{ }^\circ\text{C}$ and 12 h at $300 \text{ }^\circ\text{C}$. The sorption isotherms (quantity of argon adsorbed onto the sample surface at various pressures) were measured at 77 K and analyzed using the BET (Brunauer, Emmet, Teller) [17] and DFT (Density Functional Theory) [18,19] methods to determine the specific surface area (SSA) and pore size distribution (PSD), respectively. The analyses were performed using the Autosorb software version 1.50 supplied by Quantachrome Instruments.

The Raman analyses were performed using a Renishaw 1000 Raman micro spectrometer with a 325 nm HeCd UV laser, a 488 nm Ar+laser (frequency doubled to 244 nm) and a 780 nm diode laser in backscattering geometry. In all experiments, local sample heating induced by a laser was minimized by using a low laser beam power, defocusing the laser at the sample surface and/or using acquisition time below 2 min. In some experiments with the 244 nm UV excitation, the sample was moved during the measurements to further decrease the local heating and improve statistical reliability of the results by obtaining spectra from a larger sample volume. Obtaining high quality spectra was generally difficult due to a trade-off between the long acquisition time (or high laser power) required for the high signal-to-noise ratio and the opposite conditions needed to prevent nanocrystalline sample damage resulting from heating and oxidation in air. It should be mentioned that local heating also induces shifting of Raman peaks, which further decreases the signal-to-noise ratio and results in an asymmetric peak widening. Few measurements were performed on samples dispersed in water using the 325 nm UV laser as an excitation source. Water dissipated the induced heat and thus helped keep the local temperature low. The acquired Raman spectra did not show any significant changes even when the total collection time was as long as 30 min, allowing high quality spectra with high signal-to-noise ratio to be obtained.

TEM study was performed using a JEOL 2010F microscope at 100 kV . Low acceleration voltage was chosen in order to minimize the possible damage of non-diamond structures present in the sample. TEM samples were prepared by 10 min sonication of the powders in isopropyl alcohol and subsequent deposition of a sample drop on a lacey carbon coated copper grid.

3. Results and discussion

3.1. Specific surface area and pore size distribution

Fig. 1a shows Ar sorption isotherms of UDD samples before and after sintering. Both isotherms show a hysteresis

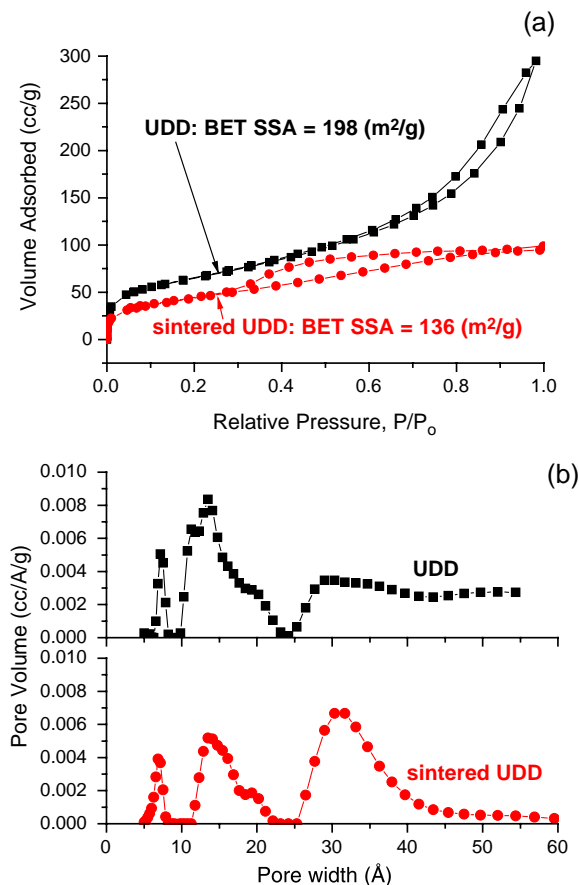


Fig. 1. Argon adsorption isotherms (a) and DFT pore size distribution (b) of UDD before and after sintering. According to BET theory, SSA of nanodiamond samples decreased from 198 to only 136 m²/g upon sintering, suggesting that sintered diamond remained a highly porous material.

and, therefore, are of type IV in the Brunauer classification [20], suggesting the presence of pores above 2 nm in both samples. The BET SSA was calculated to be 198 and 136 m²/g for as-produced and sintered nanodiamond, respectively. Simple calculations suggest that a sphere with SSA and density equal to that of the as-produced UDD should have a diameter of ~ 9.6 nm. The relatively large value obtained, compared to the nominal particle size of 6 nm reported by the manufacturer, might be explained by the underestimation of the UDD SSA due to agglomeration of nanoparticles. Although the estimation of the average grain size in sintered UDD is not possible from the sorption measurements, it is clear that the sintering process resulted in the formation of highly porous diamond with the large surface area accessible to Ar being only $\sim 30\%$ less than that of original UDD. Presumably, interconnected pores were produced between the nanocrystalline grains in the sintered powder. It is possible that non-diamond carbon present near grain boundaries was partially removed either during sintering or the acid post-treatment, creating or enlarging pores between the grains.

As mentioned earlier, the size of pores between either the agglomerated or the sintered nanodiamond particles (grains)

was evaluated using the DFT method (Fig. 1b). As the Autosorb software allowed calculations assuming only slit-shaped pores, the obtained pore size distribution might not be accurate and should be considered only an estimate. The calculated distribution of pores is similar for both samples. As expected, the average size of pores is smaller in the sintered sample due to denser grain packing. Most of the pores are below 4 nm in size. The total pore volume in the sintered sample was calculated to be ~ 0.1 cm³/g. The presence of nanopores in the sintered nanodiamond may explain its lower reported density, compared to that of diamond.

3.2. TEM analysis

Figs. 2 and 3 show TEM images of UDD before and after sintering. Lattice fringes with ~ 0.206 nm inter-planar spacing observed in both micrographs correspond to the (111) planes of diamond. Wide lines with large spacing observed in Fig. 3 originate from a Moire pattern induced by overlay of several diamond nanocrystals. Amorphous material, which may include species physisorbed on the surfaces of diamond, was observed in all samples. However, a considerably larger amount of disordered material was found in as-produced UDD. Possibly either a partial transformation of the amorphous carbon to diamond took place during the high-pressure, high temperature sintering, or additional etching or oxidation of non-diamond carbon contributed to the higher purity of the sintered diamond. No graphite particles or graphite ribbons were detected in both types of samples. However, as-prepared UDD contained considerable amount of carbon onions (Fig. 2), which were not found in the sintered powder. Possibly, onions were transformed into nanodiamond during the high-pressure high temperature sintering.

As-received UDD (Fig. 2) was agglomerated. We may speculate that during deposition of UDD onto the sample-holder, Van der Waals bonds bridged hydrophilic nanoparticles. Stronger bonding and agglomerates may also exist in the as-received nanodiamond. We did not try to make large statistic measurements to evaluate the size of diamond grains in the samples. However, after analyzing $\sim 40,000$ nm² sample area, we noticed that as-received UDD had a noticeably narrower particle size distribution and smaller average particle size, having no particles that exceeded 15 nm. In contrast, in the sintered UDD some grains were above 50 nm in size, while others were 4 nm or less. Fig. 3 shows a 27 nm grain close to the one of 4 nm in diameter. Certainly, grain coarsening took place during the sintering.

3.3. Multi-wavelength Raman analysis

As the most conventional excitation source for Raman spectroscopy, a 514 nm Ar laser (green line), is known to cause a strong fluorescence during the analysis of diamond samples, we decided to focus our efforts on using UV (244

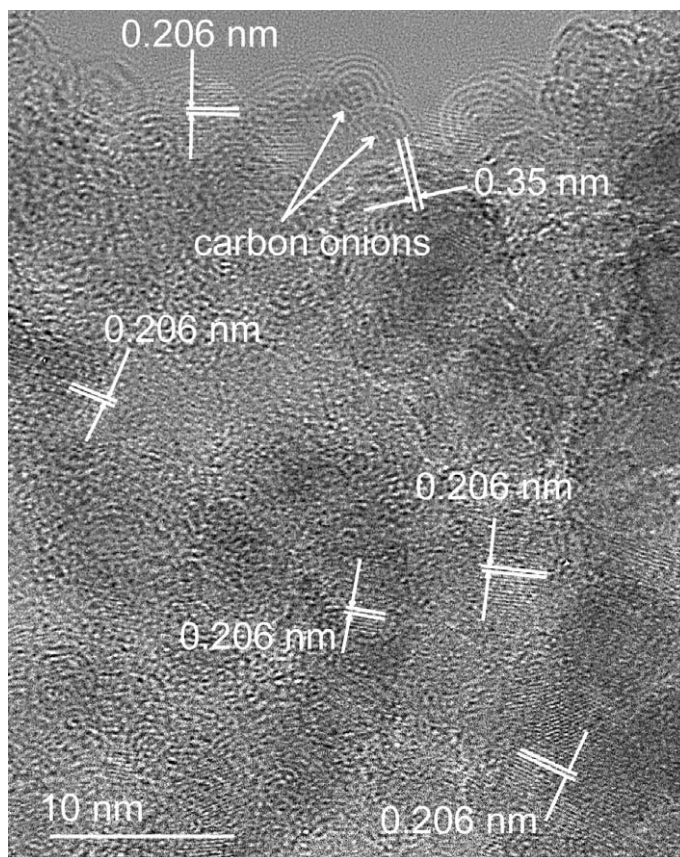


Fig. 2. HRTEM image of the agglomerated UDD. Possibly, hydrophilic nanoparticles are bridged by hydrogen or van der Waals bonds creating large agglomerates. Nanoparticles were not strongly bonded to each other within the agglomerate and particle movement was often observed in TEM. Lattice fringes with ~ 0.206 nm inter-planar distances correspond to the (111) planes of diamond. Together with nanodiamonds, amorphous carbon and carbon onions are clearly seen. The inter-planar distances between the shells of carbon onions varied in the 0.335–0.35 nm range.

and 325 nm) and near infrared (780 nm) excitations. However, our preliminary experiments showed that the Raman analysis of UDD using a 780 nm laser, which is more sensitive to sp^2 carbon, nonetheless resulted in a very high fluorescence background overlapped with the carbon bands (Fig. 4). If weak D and G (or D') bands of disordered graphite were distinguishable on the as-produced UDD, the sintered sample showed only a smooth background without carbon bands visible. The disorder-induced D and D' carbon bands are believed to be associated with a double-resonance Raman effect. A strong maximum in the phonon density of states (DOS) of graphite at ~ 1580 cm^{-1} may also contribute to D' band (see Refs. [15,21] for more detailed explanation and discussion of carbon bands).

In contrast, the UV excitations provided satisfactory Raman spectra with a very weak background present in the wavelength range of interest. The best way we found to collect the Raman spectra with a high signal-to-noise ratio was by using a gold coated sample-holder filled with DI water. Such method minimized the laser heating and oxidation of UDD during the Raman analysis. Fig. 5 shows Raman spectra of as-prepared UDD dispersed in water obtained under a 325 nm excitation. The deconvoluted spectra include a peak at ~ 1320 cm^{-1} , small peaks at

~ 730 and ~ 1050 cm^{-1} , and more prominent peaks at ~ 1250 , ~ 1560 and ~ 1640 cm^{-1} . A baseline-correction was used to provide a better fit of the observed peaks and obtain more precise peak positions. The diamond peak at ~ 1320 cm^{-1} is downshifted and broadened (FWHM of ~ 30 cm^{-1}) with respect to the single crystal diamond peak (1332 cm^{-1}). This downshift is thought to occur due to phonon confinement or changes in the phonon DOS accompanying the decrease of particles size into the nanometer range [13,22]. The position of the ~ 1050 cm^{-1} peak coincides well with the T peak of amorphous diamond discussed in Ref. [15]. Another possible contribution to this peak may come from phonon modes originating from the surface, as suggested by Praver et al. [13]. A small broad peak at ~ 1250 cm^{-1} is believed to originate from amorphous diamond [13] as suggested by the appearance of a strong maximum in the vibration DOS of diamond at similar position (~ 1250 cm^{-1}) [23]. The presence of this peak at a relatively high intensity may indicate considerable amount of amorphous diamond in UDD. The contribution of sp^2 carbon to both ~ 1050 and 1250 cm^{-1} bands is not likely but possible.

As Raman features above ~ 1360 cm^{-1} cannot be due to C-C sp^3 vibrations [24], the peaks observed in the 1500–

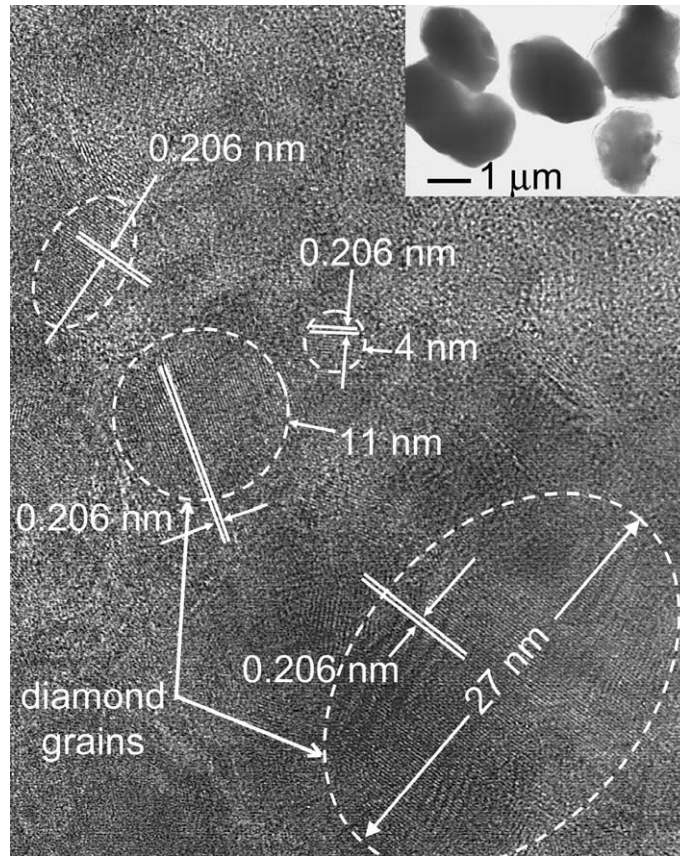


Fig. 3. TEM images of sintered UDD. A relatively large variation in grain size is clearly seen. Lattice fringes with ~ 0.206 nm inter-planar distances correspond to the (111) planes of diamond. Low magnification inset (top right) shows a typical shape and size of the sintered particles.

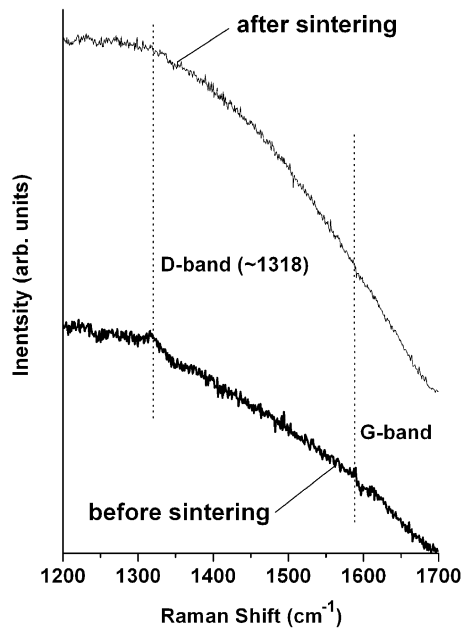


Fig. 4. Raman spectra of UDD before and after the sintering recorded with 780 nm laser excitation showing strong fluorescence with no or weak D and G bands.

1700 cm^{-1} range come from sp^2 vibrations that have considerable intensity even under the UV excitation. While the peak position at $\sim 1560\text{ cm}^{-1}$ is too high to come from the up-shifted D band of amorphous sp^2 carbon [24], another amorphous carbon band, the D' , could contribute to this peak. This peak may also come from onion-like carbon (OLC) present in the sample, as revealed by TEM observations. Due to phonon confinement, the G band in OLC may be downshifted. The downshift may also be due to tensile strains within the carbon shells [25]. As the curvature of each shell in OLC is different, the position of Raman signal should be different as well, and the overall Raman G band is expected to be broad (as observed in Fig. 5) and determined by the signals' superposition. The number of atoms in a shell increases strongly with its diameter. As such, the Raman signal coming from the outer shell should be the strongest and dominate the spectrum. The Raman signal coming from OLC was observed at $\sim 1570\text{ cm}^{-1}$ in Refs. [26] and [27], a little higher than our peak at $\sim 1560\text{ cm}^{-1}$. Such difference might be explained by a smaller average diameter of OLC in our sample. A weak peak at $\sim 700\text{--}800\text{ cm}^{-1}$ is also believed to come from OLCs. Roy et al. detected a 700 cm^{-1} peak in Raman studies of OLCs using 514.5, 633 and 785 nm excitations

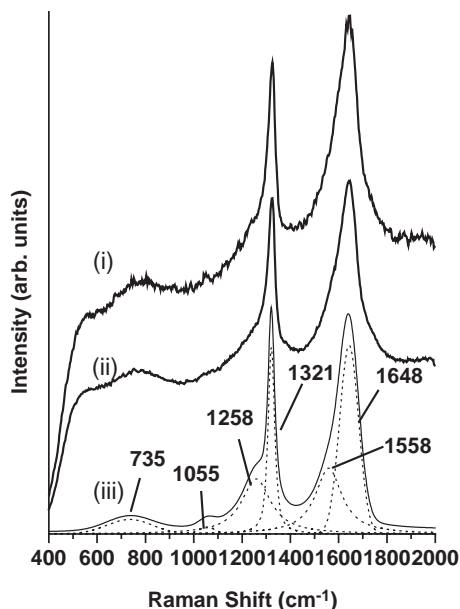


Fig. 5. Typical Raman spectra of as-produced UDD dispersed in water acquired using (i) low laser energy, (ii) high laser energy and (iii) deconvoluted after baseline-correction (325 nm excitation).

[27]. The integral intensity of this peak was 10–20 times lower than that of the G band, similar to what we observed. Relaxation of the selection rule for graphite due to the small size of OLCs and strong bending of graphene planes in their shells may cause the appearance of such a band. A peak observed at $\sim 1640\text{ cm}^{-1}$ is probably connected to amorphous sp^2 carbon present in UDD. Relatively high position of this peak might be explained by the stiffening of trigonal bonds by their tetrahedral neighbours. It is also known that the position of amorphous carbon bands may vary considerably, depending on the structure of the disordered carbon and the excitation wavelength [28–30]. Although dispersion of samples in water offers considerable advantages in signal-to-noise ratio, for better comparison with the previously published data, the rest of the discussed spectra were taken in air.

Figs. 6 and 7 compare UV Raman spectra of UDD before and after sintering taken using 325 and 244 nm excitation sources. A strong increase in the relative intensity of the diamond peak of UDD after sintering (compare typical spectra in Figs. 6a and 7a) reveals an apparent decrease in concentration of non-diamond carbon in the sample. It can also be observed that the peak at $\sim 1250\text{ cm}^{-1}$, which may be attributed to amorphous diamond, drastically diminished as well. A small peak at $\sim 1040\text{--}1060\text{ cm}^{-1}$ clearly observed in samples before sintering (see Fig. 6a and b) also disappeared (see Fig. 7a and b), which is linked to the change in surface termination of diamond grains.

As previously discussed, the downshift of the diamond peak position from 1332 cm^{-1} depends on the crystalline size of nanodiamond. A smaller average value of such a downshift observed after sintering (compare Figs. 6b,c,d and 7b,c,d) suggests the presence of larger grains in sintered

UDD, confirming the TEM observations. The spot size in Raman microspectroscopy is of the order of a micron, which makes it difficult to draw conclusions regarding the nanodiamond grain size distribution. However, the diamond peak in as-prepared UDD is located either at $\sim 1306\text{ cm}^{-1}$ or at $\sim 1320\text{--}1325\text{ cm}^{-1}$ (see Fig. 6b and c), implying possible bi-modal distribution of particle sizes. In contrast, sintered UDD showed a relatively wide and uni-modal distribution of grain sizes, resulting in Raman signal of diamond in the $1319\text{--}1329\text{ cm}^{-1}$ range (see Fig. 7b and c). Raman signal from very small diamond grains observed by TEM in the sintered sample was probably masked by a stronger signal coming from larger grains. Interestingly, the downshift of the diamond peak in sintered UDD often correlates with the increase of its full width at half maximum (FWHM) (see Fig. 7b). Such an observation suggests a macroscopically non-homogeneous distribution of nanograin sizes within the sample. In general, the as-prepared UDD sample seemed to be more homogeneous with smaller variations in the relative peak intensities (compare Figs. 6b,c and 7b,c). While most of the spectra taken on the sintered sample demonstrated low intensity of the sp^2 carbon related peaks ($1500\text{--}1700\text{ cm}^{-1}$), several spectra showed relatively strong graphitic bands, comparable to that observed in as-prepared UDD (see Fig. 7b and c).

The insignificant changes of the sp^2 carbon peak shape at various parts of both samples (before and after sintering) indicate that the same sp^2 carbon types are present everywhere within the sample. While the previously discussed spectra were acquired at one spot for each measurement, the Raman spectra of Figs. 6d and 7d where recorded while the sample was moving. As such, the obtained spectra represent an average over a larger sample area. It is worth noting that the decrease in the relative intensity of sp^2 carbon related peaks at shorter wavelengths (compare spectra in Figs. 6b and 7b taken at 325 nm to spectra in Figs. 6c and 7c taken at 244 nm excitation) is due to a resonance effect (see e.g. Ref. [15]). Due to the same effect, one may notice the downshift of the peaks related to amorphous sp^2 carbon under 244 nm excitation.

Raman data on the relative intensity of the UDD peaks (including I_D , I_T , I_G , I_{diamond}) can provide quantitative information about sample composition, degree of disorder and sp^2/sp^3 ratio. However, calibration of the Raman spectroscopy data using diamond samples with known compositions as well as a comparative electron energy loss spectroscopy (EELS), X-ray adsorption near edge spectroscopy (XANES) or nuclear magnetic resonance (NMR) studies are needed.

4. Summary

We have studied the structural changes in UDD after sintering and demonstrated the formation of high quality porous nanocrystalline diamond with a low content of non-

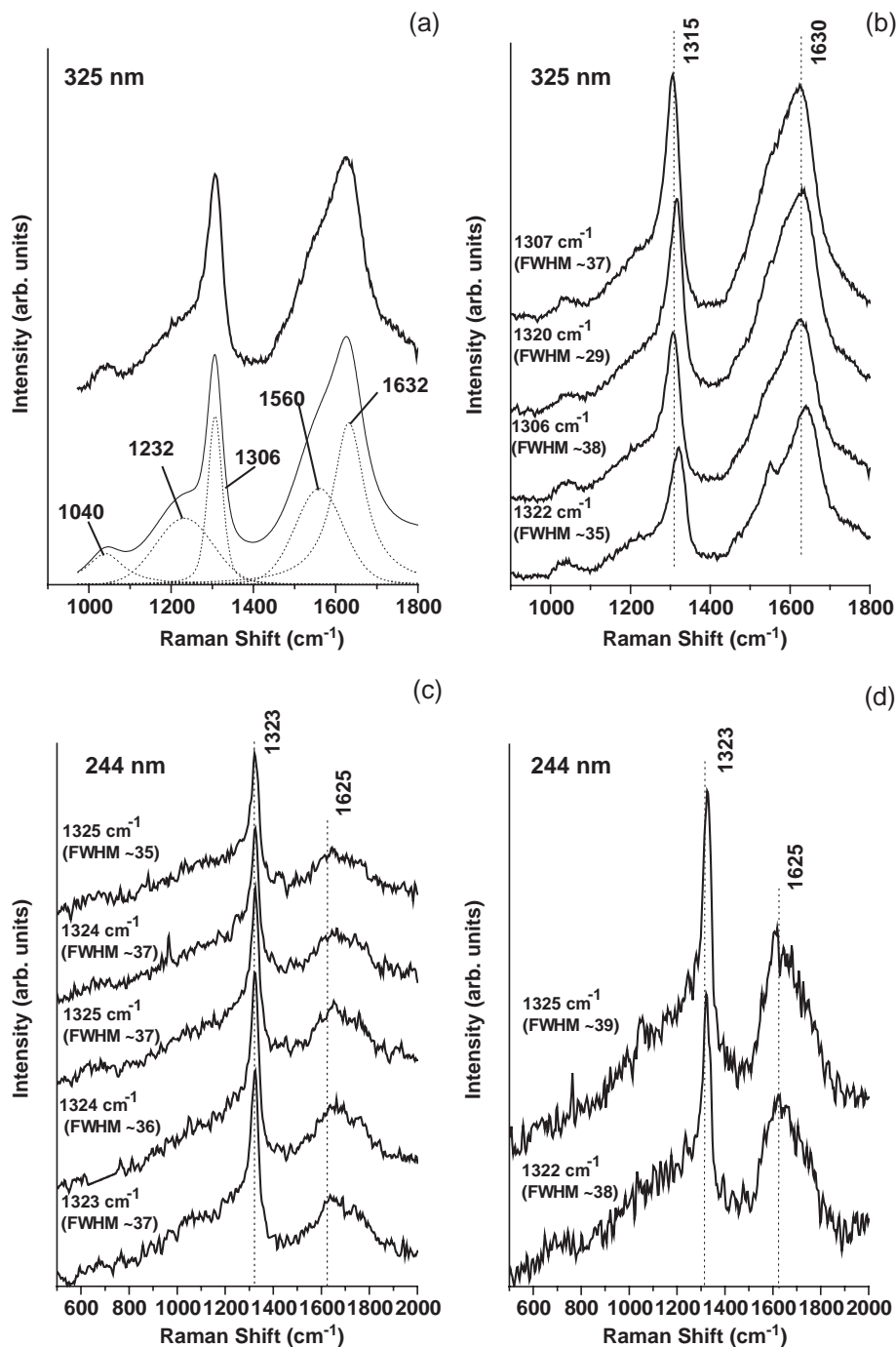


Fig. 6. Raman spectra of as-received UDD with deconvoluted peaks (a), demonstrating various contributions to the spectra (325 nm excitation); Raman spectra taken at several different sample spots using 325 nm (b) and 244 nm excitation (c), and Raman spectra measured at two different areas with sample moving (d) (244 nm excitation). An increase in the relative intensity of the diamond peak at 1305–1327 cm^{-1} under 244 nm excitation is clearly seen.

diamond phases. Argon adsorption revealed a high specific surface area (136 m^2/g) of the sintered diamond and the presence of the mesopores (<5 nm) in the produced material. A systematic study of the original and sintered UDD was performed by multi-wavelength Raman spectroscopy using 244, 325 and 780 nm excitations. Strong fluorescence background was observed under 780 nm excitation with a hardly detectable Raman signal of carbon.

UV Raman analysis of as-produced UDD showed a diamond peak at $\sim 1310\text{--}1320 \text{ cm}^{-1}$ as well as peaks observed at $\sim 700, 1050, 1250, 1560, \text{ and } 1630 \text{ cm}^{-1}$. Potential contributions of sp^2 and sp^3 amorphous carbon as well as carbon onions present in as-produced UDD to the Raman spectra were discussed. In general, UV Raman of the sintered UDD showed considerable decrease in the relative intensities of the non-diamond peaks. However, higher

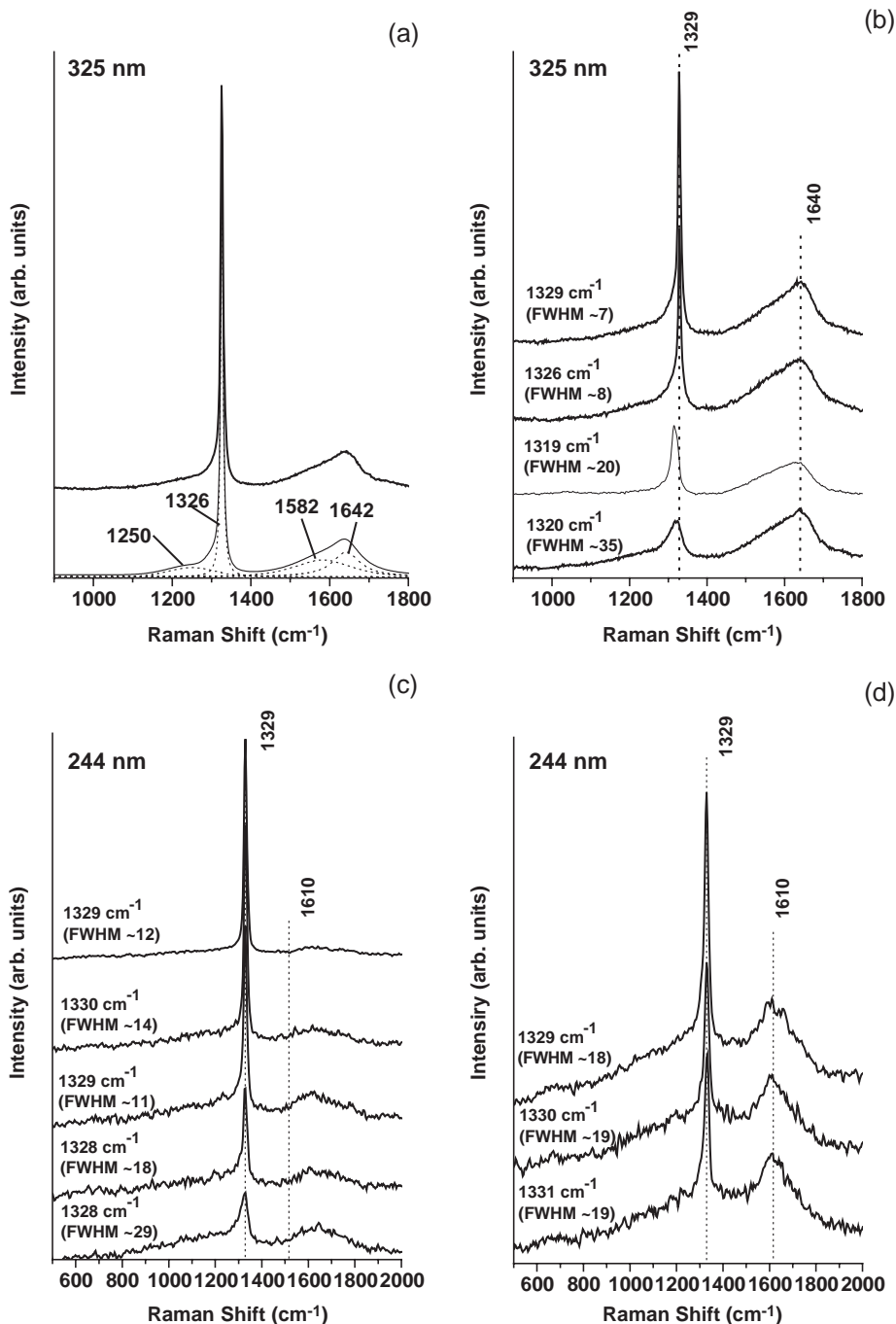


Fig. 7. Raman spectra of sintered UDD with deconvoluted peaks (a), demonstrating various contributions to the spectra (325 nm excitation); Raman spectra taken at several different sample spots using 325 nm (b) and 244 nm excitation (c), revealing non-uniformity of the sample and variation of the relative peak intensities; and Raman spectra measured at three different areas with sample moving (d) (244 nm excitation).

average position and stronger variations on the relative intensities of the diamond peak in the sintered sample, compared to the original UDD, suggested partial grain coarsening and non-uniform diamond purification as a result of sintering. High resolution TEM showed the presence of carbon onions and a considerable amount of amorphous carbon in the original UDD samples and a noticeably smaller amount of amorphous material and no carbon onions in the sintered UDD. An increase in average grain

size and larger variation in the grain size of the sintered UDD were also seen by the TEM.

References

- [1] V.Y. Dolmatov, *Russ. Chem. Rev.* 70 (2001) 607.
- [2] O.A. Shenderova, V.V. Zhimov, D.W. Brenner, *CRC Crit. Rev. Solid State Mater. Sci.* 27 (3–4) (2004) 227.

- [3] A.L. Vereschagin, Detonation Nanodiamonds, Altai State Technical University (in Russian), Barnaul, Russia, 2001.
- [4] V.V. Danilenko, Synthesis and Sintering of Diamond by Explosion, Energoatomizdat (in Russian), Moscow, Russia, 2003.
- [5] G. Post, et al., *Russ. J. Appl. Chem.* 75 (5) (2002) 755.
- [6] G.P. Bogatyreva, et al., in: Y. Gogotsi, I. Uvarova (Eds.), *Nanostructured Materials and Coatings for Biomedical and Sensor Applications*, Kluwer Academic Publishers, Dordrecht, 2002, p. 111.
- [7] G.P. Bogatyreva, M.A. Marinich, V.L. Gvyazdovskaya, *Diamond Relat. Mater.* 9 (2000) 2002.
- [8] Y. Gogotsi, et al., *Nature* 411 (2001) 283.
- [9] R.J. Nemanich, et al., *J. Vac. Sci. Technol., A, Vac. Surf. Films* 6 (3) (1988) 1783.
- [10] S. Praver, R.J. Raman, *Philos. Trans. R. Soc. Lond., A* 362 (2004) 2477.
- [11] G. Morell, et al., *Diamond Relat. Mater.* 7 (7) (1998) 1029.
- [12] L.C. Nistor, et al., *Diamond Relat. Mater.* 6 (1) (1997) 159.
- [13] S. Praver, et al., *Chem. Phys. Lett.* 332 (2000) 93.
- [14] M. Yoshikawa, et al., *Appl. Phys. Lett.* 67 (5) (1995) 694.
- [15] A.C. Ferrari, J. Robertson, *Phil. Trans. R. Soc. Lond., A* 362 (2004) 2267.
- [16] G.P. Bogatyreva, M.A. Marinich, E.V. Ishchenko, *International Conference New Diamond Science and Technology, ICNDST-8*, The University of Melbourne, Australia, 2002.
- [17] S. Brunauer, P. Emmett, E. Teller, *J. Am. Chem. Soc.* 60 (1938) 309.
- [18] R. Evans, *Adv. Phys.* 28 (2) (1979) 143.
- [19] P.I. Ravikovitch, A.V. Neimark, *Colloids Surf.* 187–188 (2001) 11.
- [20] P.A. Webb, C. Orr, *Analytical Methods in Fine Particle Technology*, Micromeritics Instrument Corporation, 1997.
- [21] P. Tan, S. Dimovski, Y. Gogotsi, *Philos. Trans. R. Soc. Lond., A* 362 (2004) 2289.
- [22] J.W. Ager, D.K. Veirs, G.M. Rosenblatt, *Phys. Rev., B* 43 (8) (1991) 6491.
- [23] C.Z. Wang, K.M. Ho, *Phys. Rev. Lett.* 71 (1993) 1184.
- [24] A.C. Ferrari, J. Robertson, *Phys. Rev., B* 61 (2000) 14095.
- [25] P. Lespade, R. Al-Jishi, M.S. Dresselhaus, *Carbon* 20 (5) (1982) 427.
- [26] E.D. Obraztsova, et al., *Carbon* 36 (5–6) (1998) 821.
- [27] D. Roy, et al., *Chem. Phys. Lett.* 273 (2003) 52.
- [28] A.C. Ferrari, *Diamond Relat. Mater.* 11 (2002) 1053.
- [29] F. Negri, et al., *J. Chem. Phys.* 120 (24) (2004) 11889.
- [30] A.C. Ferrari, J. Robertson, *Phys. Rev., B* 64 (2001) 075414.